

p53-cofactor JMY is a multifunctional actin nucleation factor

J. Bradley Zuchero¹, Amanda S. Coutts², Margot E. Quinlan³, Nicholas B. La Thangue² and R. Dyche Mullins^{1,4}

Many cellular structures are assembled from networks of actin filaments, and the architecture of these networks depends on the mechanism by which the filaments are formed. Several classes of proteins are known to assemble new filaments, including the Arp2/3 complex, which creates branched filament networks, and Spire, which creates unbranched filaments^{1,2}. We find that JMY, a vertebrate protein first identified as a transcriptional co-activator of p53, combines these two nucleating activities by both activating Arp2/3 and assembling filaments directly using a Spire-like mechanism. Increased levels of JMY expression enhance motility, whereas loss of JMY slows cell migration. When slowly migrating HL-60 cells are differentiated into highly motile neutrophil-like cells, JMY moves from the nucleus to the cytoplasm and is concentrated at the leading edge. Thus, JMY represents a new class of multifunctional actin assembly factor whose activity is regulated, at least in part, by sequestration in the nucleus.

By searching genome databases for sequences related to the Wiskott–Aldrich syndrome protein (WASP) Homology 2 (WH2) domain we discovered a potential Arp2/3-activating sequence, WWWCA, in the vertebrate protein JMY (Fig. 1a). This sequence is composed of three tandem repeats of the actin-monomer-binding WH2 domain (WWW), a central domain (C) that binds actin and Arp2/3, and an Arp2/3-binding acidic domain (A). These sequence elements, first identified in WASP-family proteins^{1,3}, collaborate in activating Arp2/3. The identification of these elements in JMY was surprising, because JMY localizes primarily to the nucleus and was originally discovered as a binding partner of p300, a co-activator for many transcription factors, including the tumour suppressor p53 (ref. 4). In fibroblasts JMY accumulates in the nucleus in response to DNA damage, where it enhances the p53-dependent transcription of pro-apoptotic genes^{4,5}.

To determine whether JMY also has a function in the assembly of the actin cytoskeleton, we tested the effect of JMY expression on actin organization *in vivo*. Overexpression of JMY in human U2OS cells induces the formation of elongated actin filament structures that co-localize with

JMY (Fig. 1b), in a similar manner to overexpression of WASP-family proteins and the actin nucleation factor Spire^{2,6}. Truncation mutants demonstrate that the WH2 cluster is required for this effect but, curiously, the Arp2/3-binding CA domain is not (Supplementary Information, Fig. S1). Expression of the carboxy-terminal region of JMY fused to green fluorescent protein (GFP-PWWCA) produces a linear, dose-dependent increase in the cellular concentration of filamentous actin (Fig. 1c) as judged by correlating Alexa Fluor 568-phalloidin staining with GFP fluorescence ($n = 457$; Fig. 1d). In contrast, expressing GFP alone has no significant effect on cellular levels of filamentous actin ($n = 458$; Fig. 1d; Supplementary Information, Fig. S1).

To study how JMY affects actin assembly *in vitro*, we first verified that all three putative WH2 domains (W_a , W_b and W_c , from amino terminus to carboxy terminus) bind monomeric actin (Supplementary Information, Fig. S2). JMY activates Arp2/3 *in vitro*, as determined by pyrene-actin polymerization assays using a C-terminal fragment of JMY (WWWCA) (Fig. 1e; $t_{1/2}$ (JMY + actin + Arp2/3) = 42.2 ± 2.3 s, versus $t_{1/2}$ (actin + Arp2/3) = $1,193 \pm 28$ s (mean \pm s.e.m.)). JMY WWWCA also induces rapid actin polymerization in the absence of Arp2/3 (Fig. 1e; $t_{1/2}$ = 188.5 ± 4.4 s). The JMY-dependent increase in polymerization rate is dose-dependent, both with and without Arp2/3 (Fig. 1f). This result is quite surprising and distinguishes JMY from all other proteins known to activate Arp2/3. N-WASP WWWCA, for example, activates Arp2/3 to a similar extent as JMY but does not accelerate polymerization in the absence of Arp2/3 (Fig. 1e).

By itself JMY could accelerate actin assembly by nucleating new filaments, by increasing the rate of filament elongation, or by severing existing filaments to create new barbed ends^{2,7}. JMY does not affect the elongation of preformed filaments, arguing that it neither accelerates elongation nor severs, but rather nucleates new filaments (Supplementary Information, Fig. S3a–c). Indeed, we observe more than 12-fold more filaments in the presence of JMY WWWCA compared with actin alone (Fig. 2a, b). In the presence of Arp2/3, JMY WWWCA produces branched filaments, which is consistent with nucleation by Arp2/3 (Fig. 2c, left panel), whereas, by itself, JMY nucleates unbranched filaments (Fig. 2a). In assembly reactions, filament length is inversely

¹Cellular and Molecular Pharmacology, University of California, San Francisco, California 94158, USA. ²Laboratory of Cancer Biology, Division of Medical Sciences, University of Oxford, Oxford OX3 9DU, UK. ³Chemistry and Biochemistry, University of California, Los Angeles, California 90095, USA. ⁴Correspondence should be addressed to R.D.M. (e-mail: dyche@mullinslab.ucsf.edu)

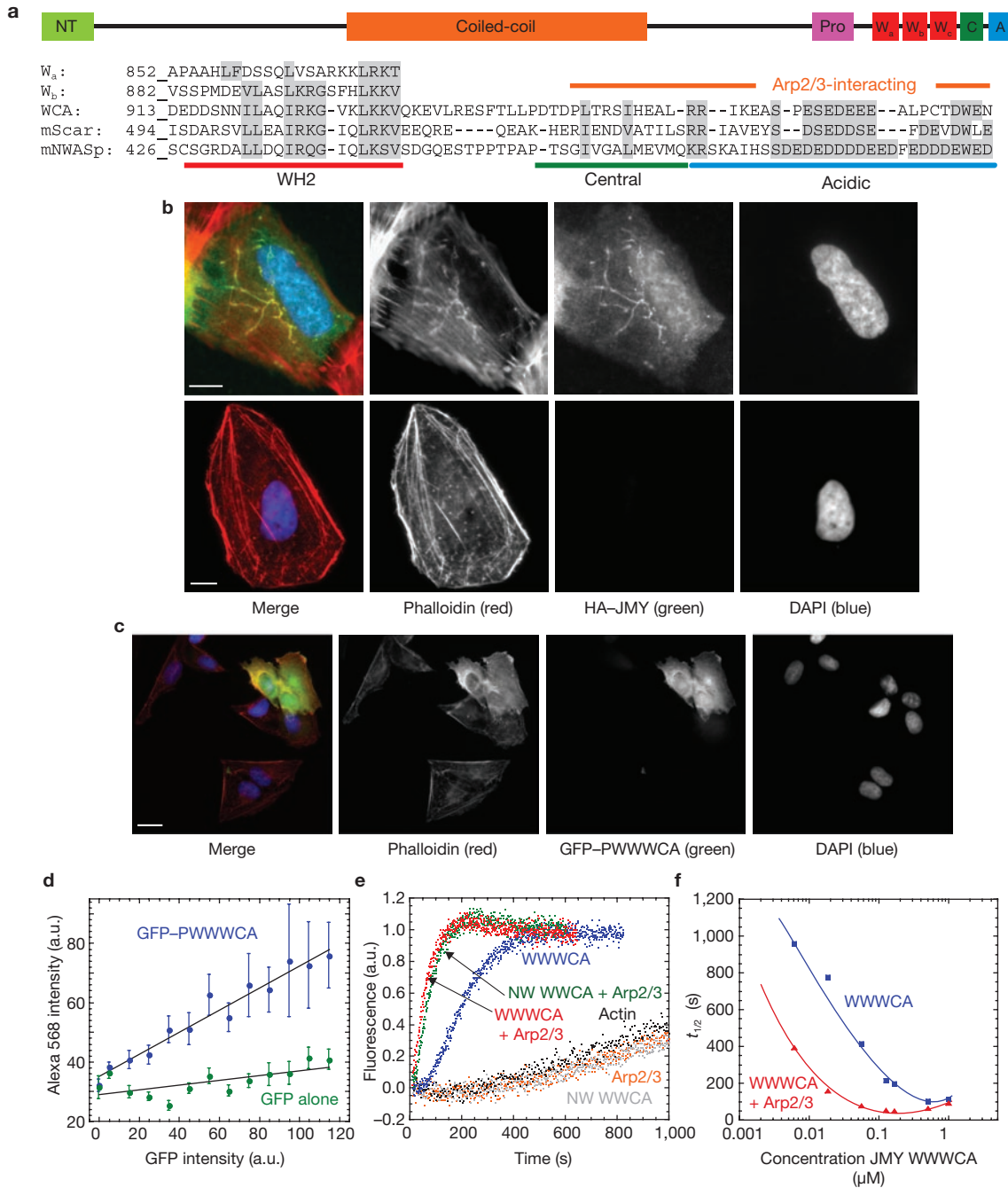


Figure 1 JMY nucleates actin filaments and activates the Arp2/3 complex. **(a)** Domain structure of JMY. The C terminus of JMY is homologous to activators of Arp2/3. A poly-proline (P) domain²⁸ is followed by three tandem actin-monomer-binding WH2 domains (W_a, W_b and W_c), a central domain (C) binding actin and Arp2/3, and an Arp2/3-binding acidic domain (A). Alignment shows individual WH2 domains of JMY, and compares the sequences of the WCA regions of JMY, Scar and N-WASp. JMY WCA is 28% identical to N-WASp WCA (ClustalW), and residues putatively involved in binding actin and Arp2/3 (refs 29, 30) are 100% conserved between all available JMY sequences. **(b)** Expression of haemagglutinin (HA)-tagged JMY (top panels; revealed by indirect immunofluorescence of HA, green) in U2OS cells induces the formation of filamentous actin structures (revealed with Alexa Fluor 568-phalloidin, red). These elongated actin structures co-localize with JMY and are not seen in untransfected cells (bottom panels). Nuclei were revealed with DAPI (blue). Scale bar, 10 μ m. **(c)** Expression of GFP-PWWWCA (green) in U2OS cells increases cellular F-actin content (Alexa Fluor

568-phalloidin, red). **(d)** Quantification of the increase in F-actin induced by GFP-PWWWCA expression. Phalloidin intensity was plotted as a function of GFP-PWWWCA intensity and shows a linear increase in F-actin content with increased expression of GFP-PWWWCA ($n = 457$). In contrast, expressing GFP alone has only a minor effect on the red intensity detected, probably due to a small amount of bleed-through ($n = 458$). a.u., arbitrary units. Error bars indicate s.e.m. **(e)** Pyrene-actin polymerization assays show that JMY WWWCA both activates Arp2/3 and nucleates actin in the absence of Arp2/3 (red and blue traces). N-WASp (NW) WWCA activates Arp2/3 (green), but does not nucleate actin on its own (grey). **(f)** Intrinsic nucleation and activation of Arp2/3 by WWWCA are dose-dependent. Pyrene-actin polymerization assays were conducted in the absence (blue) or presence (red) of Arp2/3, with increasing concentrations of JMY WWWCA. Time to half-maximal polymerization ($t_{1/2}$) was plotted as a function of WWWCA concentration. Pyrene-actin polymerization assays were performed in 1 \times KMEI and contained 2 μ M actin, 167 nM JMY or N-WASp, and 2.5 nM Arp2/3, where noted.

proportional to the rate of nucleation, and filaments made in the presence of JMY are shorter than those made with actin alone. Arp2/3-nucleated filaments are even shorter (Fig. 2d). JMY produces twice as many branches per micrometre as Scar1/WAVE1 (Fig. 2e), which is consistent with JMY inducing a faster rate of Arp2/3 activation than Scar.

Some proteins that cap barbed ends *in vivo* (for example capping protein) nucleate filaments that elongate from their pointed end *in vitro*⁸. To determine whether JMY caps barbed ends, we made filaments and depolymerized them in the presence of JMY WWCA. JMY does not inhibit disassembly, arguing that it does not cap barbed ends but instead promotes polymerization by nucleating new filaments that elongate from their barbed ends (Supplementary Information, Fig. S3d, e). Direct nucleation seems to explain the unexpected ability of JMY to induce actin assembly *in vivo* in the absence of the Arp2/3-binding CA domain (Supplementary Information, Fig. S1).

We proposed that, in a similar manner to Spire², JMY uses its tandem WH2 domains to nucleate new filaments. We tested the activity of constructs consisting of either all three WH2 domains (JMY WWW) or the two C-terminal WH2 domains (JMY W_bW_c). JMY WWW nucleates actin as well as WWWCA, indicating that the CA region has no function in direct nucleation (Fig. 2f). Moreover, addition of Arp2/3 to JMY WWW does not further increase the rate of polymerization (Fig. 2f). As with Spire, the two C-terminal WH2 domains (JMY W_bW_c) are sufficient for nucleation, but all three JMY WH2 domains are required for maximal activity (Supplementary Information, Fig. S3h, i).

In contrast, a fragment composed of a single WH2 domain (W_c) and the CA domains (JMY WCA) activates Arp2/3 but does not nucleate filaments on its own (Fig. 2g). JMY contains a conserved tryptophan residue known to be important for Arp2/3 binding in all WASp-family proteins⁹. Replacing this tryptophan residue with alanine in JMY decreases the activation of Arp2/3 without affecting intrinsic nucleation activity (Supplementary Information, Fig. S3j). These results suggest that nucleation and Arp2/3 activation are separable activities, and that JMY activates Arp2/3 by the same mechanism as WASp-family proteins.

Similarities in the sequences and activities of JMY and Spire suggested that the two proteins nucleate filaments by a common mechanism. We compared the kinetics of nucleation by JMY and Spire over a range of actin concentrations. At all concentrations of actin tested, JMY and Spire had nearly identical kinetics (Supplementary Information, Fig. S3k, l). In addition, similarly to Spire, high concentrations of JMY sequester actin monomers (Supplementary Information, Fig. S3m, n). Unlike Spire, however, JMY WWCA does not prevent the dissociation of monomers from the pointed end of filaments (Supplementary Information, Fig. S3f, g). It is possible that the full-length JMY interacts with filament ends, but this is not required for nucleation.

Spire nucleates actin by stitching monomers together with tandem WH2 domains and a novel actin-binding motif (previously called Linker 3; ref. 2) that we designate the monomer binding linker (MBL). Spire-MBL, a short (about 15-residue) sequence connecting the third and fourth WH2 domains, is sufficient to promote weak nucleation². We compared the sequences of Spire-MBL with the region between the two C-terminal WH2 domains of JMY (W_b and W_c) and N-WASp. Most residues conserved between Spire homologues are also conserved in JMY, but not in N-WASp (Fig. 3a). Another WH2-containing nucleation factor, Cordon Bleu (Cobl), is thought to operate by a different mechanism¹⁰;

consistent with this was the fact that we saw no conservation between the linker regions of Cobl and Spire (Fig. 3a).

Do JMY and Spire nucleate actin by the same mechanism? We replaced the JMY linker with a set of glycine-serine repeats (JMY W_bW_c(gs5)) and compared it with a similar Spire mutant (Spire CD(gs5)). JMY W_bW_c(gs5) has a modest defect in nucleation, whereas replacing the linker in Spire has a more pronounced effect (Fig. 3b, d; Supplementary Information, Fig. S3o). Interestingly, inserting either the JMY-MBL or Spire-MBL between the N-WASp WH2 domains (NW WJW or WSW) converted N-WASp into a nucleator (Fig. 3c, d; Supplementary Information, Fig. S3p), whereas inserting a flexible linker (NW WW(gs5)) did not (Fig. 3b, d). NW WJW and WSW do not nucleate as well as JMY or Spire. Thus, nucleation by JMY and Spire requires unique properties of both the linker (MBL) and the WH2 domains (Fig. 3e).

To investigate its role in actin assembly *in vivo*, we determined the localization of JMY in multiple cell types. JMY is primarily nuclear in mouse embryonic fibroblasts, B16-F10 mouse melanoma cells, NIH 3T3 cells and primary rat neurons (Supplementary Information, Fig. S4, and data not shown). In ruffling B16-F10 cells, we observed a small fraction of JMY co-localized with actin filaments at the leading edge (Supplementary Information, Fig. S4b). In highly motile, primary human neutrophils, JMY was almost entirely excluded from the nucleus and co-localized with filaments at the leading edge (Fig. 4d). JMY does not bind actin filaments *in vitro*, so this localization does not simply reflect the direct interaction of JMY with filaments (Supplementary Information, Fig. S4d).

Our localization studies suggest that the presence of JMY at the leading edge correlates with motility. To test this further, we investigated JMY expression and localization in HL-60 cells, which can exist as non-motile, relatively undifferentiated cells or be induced to differentiate into highly motile cells¹¹. In undifferentiated HL-60 cells, JMY is primarily nuclear and does not co-localize with filaments (primarily nuclear in 91% of cells, $n = 246$; Fig. 4a; Supplementary Information, Fig. 5). The addition of 1.3% dimethylsulphoxide (DMSO) to the culture medium induces differentiation into highly motile cells that polarize and undergo chemotaxis. During differentiation, JMY localization shifts markedly, becoming almost entirely cytoplasmic. This shift occurs about two days before cells are competent to polarize in response to formyl peptide chemoattractant (fMLP; Supplementary Information, Fig. S5c). In differentiated cells, JMY co-localizes with filamentous actin in the cell cortex (cytoplasmic in 94%, nuclear in 6%, $n = 212$; Fig. 4b), and on addition of fMLP, JMY localizes strongly to the leading edge, where it overlaps with filamentous actin (88% of polarized cells, $n = 311$; Fig. 4c; Supplementary Information, Fig. S5d). A comparison of JMY staining with the location of soluble GFP in polarized cells shows that enrichment of JMY at the leading edge is not a volume artefact (Supplementary Information, Fig. S5e–g). These data suggest that translocation of JMY to the cytosol has a function in building the leading edge. Interestingly, expression of JMY's nuclear binding partner p300 disappears when HL-60 cells are differentiated, suggesting that the nuclear (p300/p53-dependent transcription) and cytoplasmic (actin nucleation) roles of JMY are regulated by separate pathways (Fig. 4e).

To examine the role of JMY in cell motility, we stably expressed GFP-JMY and GFP-JMYΔCA in U2OS cells, grew monolayers, scratched them, and monitored wound healing over time¹². Cells expressing GFP-JMY migrated 17% faster than wild-type cells ($n = 3$;

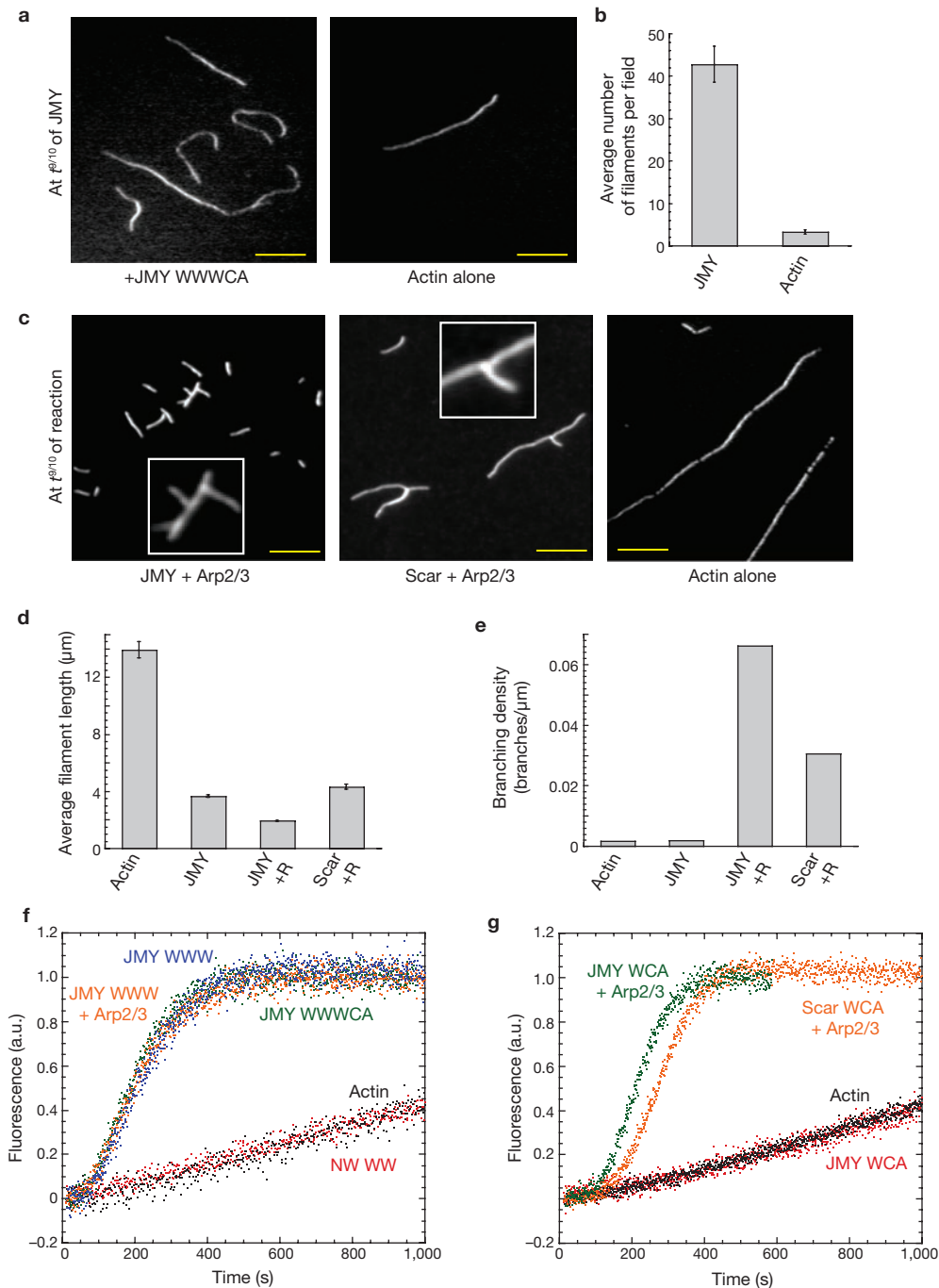


Figure 2 Mechanistic dissection of JMY. **(a)** JMY nucleates unbranched filaments and increases the number of filaments over actin alone. Filaments made in the presence (left) or absence (right) of 167 nM JMY WWWCA were fixed with Alexa Fluor 488 phalloidin and Latrunculin B at 6 min ($t^{9/10}$ of JMY WWWCA reaction) before dilution and spotting onto poly-(L-lysine) coverslips^{2,24}. Scale bars, 5 μm . **(b)** Quantification of filaments per field in images from **a** demonstrates that JMY nucleates new filaments (JMY, 42.7 ± 4.2 filaments per micrometre, $n = 35$ fields; actin alone, 3.2 ± 0.5 filaments per micrometre, $n = 30$ fields). Error bars indicate s.e.m. **(c)** Filaments prepared as in **a**, in the presence of JMY plus Arp2/3 (left), Scar plus Arp2/3 (centre) or actin alone (right). The concentration of filaments was kept constant by arresting reactions at their individual $t^{9/10}$ values (see Methods). Filaments nucleated in the presence of JMY and Arp2/3 are branched, which is consistent with JMY activating Arp2/3, as are filaments made in the presence of Scar

and Arp2/3. The shorter, more abundant filaments seen here are due to Arp2/3 nucleating actin more rapidly than intrinsic nucleation by JMY. **(d)** Quantification of filament length at $t^{9/10}$. The rate of nucleation is inversely proportional to the length of filament (rate: JMY+Arp2/3 > JMY > Scar+Arp2/3 >> actin alone). Error bars indicate s.e.m. **(e)** Quantification of filament branching in each condition. $n > 300$ filaments per condition. **(f)** Tandem WH2 domains from JMY are sufficient for actin nucleation. Actin polymerization is as fast with WWW as it is with WWWCA. WWW lacks the Arp2/3-binding CA domain, so adding Arp2/3 to WWW does not accelerate polymerization over WWW alone. N-WASp WW does not nucleate actin. **(g)** JMY WCA is sufficient to activate Arp2/3 but does not nucleate actin. The rate of actin polymerization in the presence of JMY WCA and Arp2/3 is similar to reactions containing Scar WCA and Arp2/3. In the absence of Arp2/3, JMY WCA has no effect on actin polymerization. Experimental conditions were as in Fig. 1.

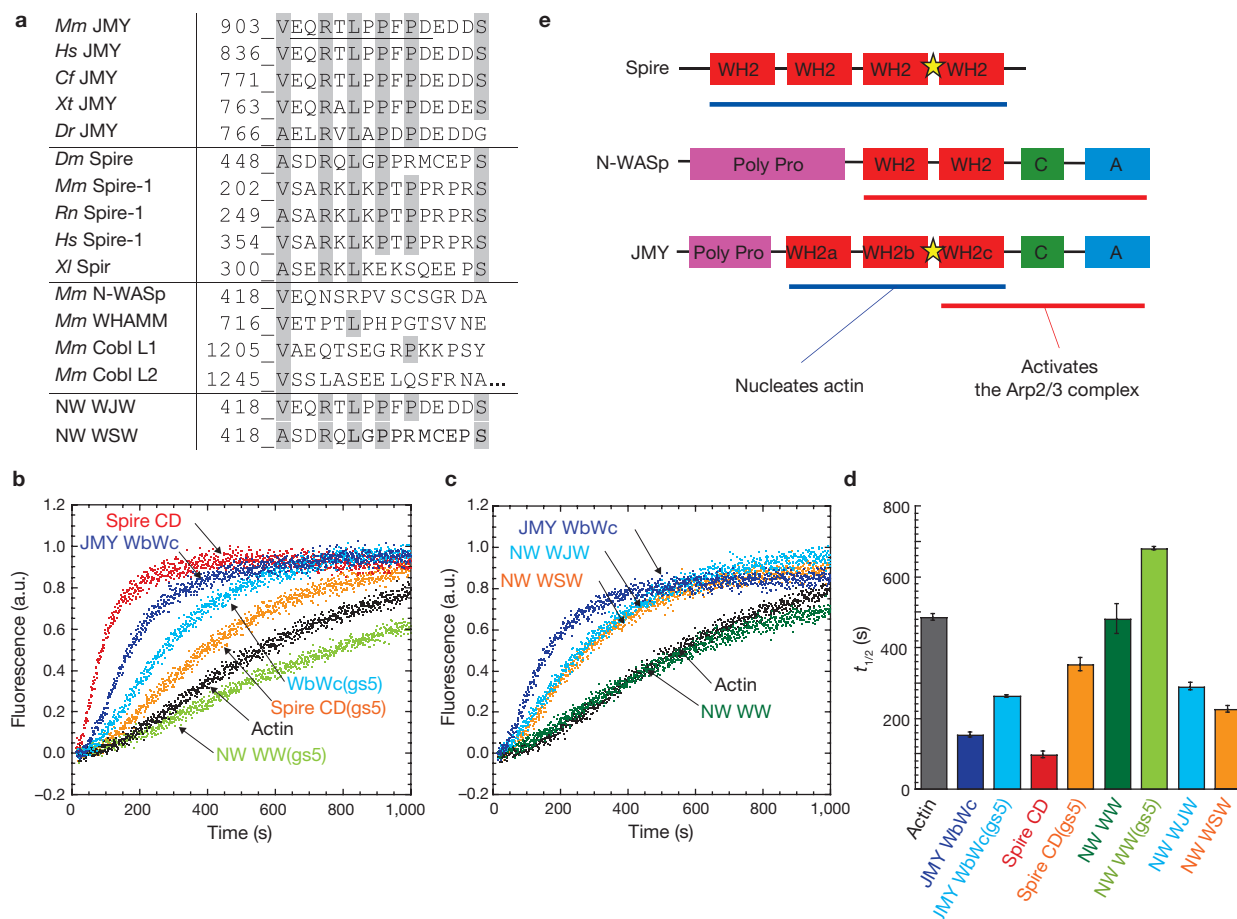


Figure 3 JMY nucleates actin by the same mechanism as Spire. **(a)** The region between JMY W_b and W_c is homologous to the short actin nucleation motif from Spire (monomer-binding linker, MBL). The figure shows an alignment between Spire-MBL and the same region of JMY (mJMY residues 903–917) with homologous residues coloured grey. The MBL sequence is not homologous to the analogous position in N-WASp, WHAMM³¹ or Cordon Bleu¹⁰. The position of the glycine-serine repeats in **b** is underlined, and the sequences of N-WASp gain-of-function mutations (NW WJW and WSW) in **c** are shown. Organisms: *Mm*, *Mus musculus*; *Hs*, *Homo sapiens*; *Cf*, *Canis familiaris*; *Xt*, *Xenopus tropicalis*; *Dr*, *Danio rerio*; *Dm*, *Drosophila melanogaster*; *Rn*, *Rattus norvegicus*; *Xl*, *Xenopus laevis*. **(b)** JMY-MBL is important for actin nucleation. Replacing the MBL in JMY W_bW_c and Spire CD (the two C-terminal WH2 domains in Spire) with a flexible linker

$P < 0.003$; Fig. 5a, b; Supplementary Information, Fig. S6). In contrast, cells expressing GFP-JMY Δ CA migrated at the same rate as wild-type cells (GFP-JMY, $43.8 \pm 1.6 \mu\text{m h}^{-1}$; GFP-JMY Δ CA, $38.5 \pm 1.7 \mu\text{m h}^{-1}$; wild-type, $37.5 \pm 1.0 \mu\text{m h}^{-1}$), suggesting that JMY requires its Arp2/3-activating activity to enhance motility.

We next knocked down JMY expression in cultured U2OS and HEK 293 cells by RNA-mediated interference (RNAi). Western blotting shows that RNAi was efficient (Fig. 5e; Supplementary Information, Fig. S6). In both cell lines, knockdown of JMY expression significantly slows the rate of wound healing (Fig. 5c, d; Supplementary Information, Fig. S6). In the first 6 h, cells treated with JMY small interfering RNA (siRNA) moved 38.0% more slowly than control U2OS cells ($n = 4$; $P < 0.05$). By 24 h, control cells migrated fully into the wound, whereas cells treated with JMY siRNA migrated only 86% of the distance (Fig. 5a, b; $n = 4$). Control HEK 293 cells migrated 92%

of glycine-serine repeats (gs5) causes a nucleation defect in both JMY and Spire. The analogous N-WASp mutant does not promote nucleation, but instead inhibits spontaneous polymerization. **(c)** Gain of function. Replacing the linker region between the WH2 domains of N-WASp WW with JMY-MBL or Spire-MBL (NW WJW or WSW) converts N-WASp into a weak actin nucleator. This shows that JMY-MBL and Spire-MBL are sufficient for nucleation. Mutated residues of WJW and WSW are shown in **a**. Reactions in **b** and **c** contained $4 \mu\text{M}$ actin. Experimental conditions were as in Fig. 1. **(d)** $t_{1/2}$ values of reactions from **b** and **c**. Reactions were repeated more than three times each. Error bars indicate s.e.m. **(e)** Actin nucleation and activation of Arp2/3 are distinct activities of JMY that overlap spatially. Tandem JMY WH2 domains and the MBL (star) nucleate actin, similarly to Spire, and JMY WCA activates Arp2/3, similarly to N-WASp and Scar.

of the distance by 24 h, in contrast with 60% for cells treated with JMY siRNA (Supplementary Information, Fig. S6; $n = 7$).

Defects in wound healing could be caused by (1) reduced actin assembly, (2) altered transcription, (3) reduced cell division or increased apoptosis, or (4) off-target effects of the siRNA. Consistent with the first explanation was our observation that that JMY knockdown cells contained $11.4 \pm 0.4\%$ ($n = 396$, $P < 0.03$) less filamentous actin than wild-type cells (Fig. 5f). Loss of either p53 or p300, both of which are required for all JMY's known transcriptional effects, leads to increased cell migration^{13–15}, which is inconsistent with transcriptional effects on motility. In addition, less than 5% of cells close to the wound divide in the first 6 h of the assay, making it unlikely that cell division contributes to the observed defect. Knockdown of JMY was shown to decrease apoptosis⁵, ruling out the third explanation. To address possible off-target effects, we used three different siRNAs, from different regions of

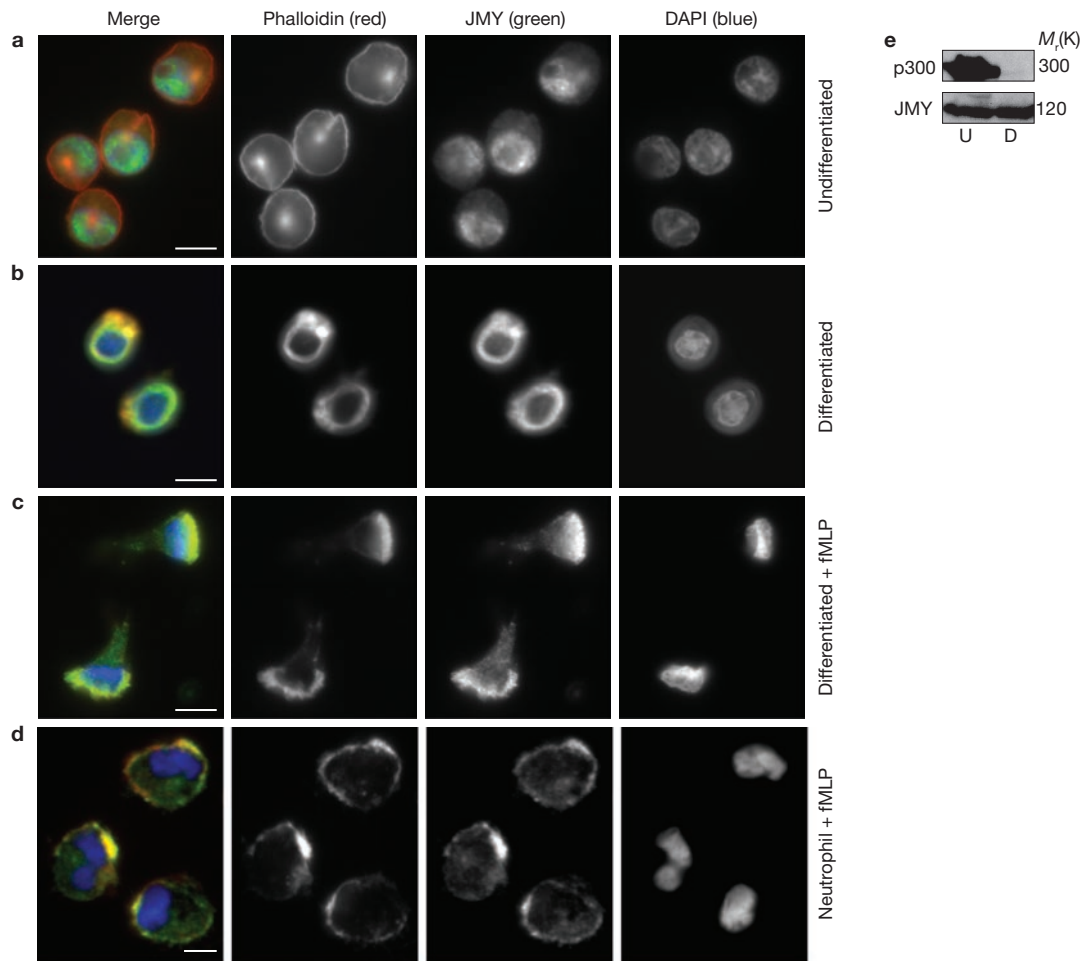


Figure 4 JMY localizes to the leading edge of motile cells. **(a–c)** Redistribution of JMY from the nucleus to the leading edge in HL-60 cells. **(a)** JMY is primarily nuclear in undifferentiated HL-60 cells. **(b)** After differentiation into motile cells by being cultured in 1.3% DMSO for 5–7 days, JMY co-localizes with filamentous actin in the cytoplasm. **(c)** Differentiated HL-60 cells were polarized by exposure to 100 nM fMLP, a chemoattractant. JMY is distributed throughout the cytoplasm, where it co-localizes strongly with filamentous actin at the leading edge.

Cells were fixed and stained with Alexa Fluor 568-phalloidin (red), anti-JMY (green) and DAPI (blue). Scale bars, 10 μ m. **(d)** Human primary neutrophils were obtained by finger prick²⁶, stimulated with 20 nM fMLP, and fixed and stained as above. JMY (green) co-localizes with filamentous actin (red) at the leading edge. Scale bar, 5 μ m. **(e)** Western blots of JMY and its binding partner p300 in undifferentiated (U) and differentiated (D) HL-60 cells. p300 is expressed in undifferentiated, but not differentiated, HL-60 cells.

the human JMY gene, to knock down expression in HEK 293 cells. All three caused migration defects (Supplementary Information, Fig. S6g), whereas a control siRNA had no effect.

We next tested whether JMY localizes to the leading edge of U2OS cells during migration in response to a wound, as seen in highly motile HL-60 cells. We fixed and stained U2OS cells 15 min after wounding, as well as cells in subconfluent and non-wounded cultures. Although most of JMY was nuclear in these cells, we also observed both endogenous JMY and GFP-JMY co-localized with filamentous actin at the leading edge (Fig. 5g; Supplementary Information, Fig. S4c), both in cells adjacent to a wound and in ruffling edges of subconfluent cells (data not shown). Thus, even in cells in which JMY is predominantly nuclear, a fraction of the protein can influence actin assembly at the leading edge and promote migration.

JMY combines an unusual set of activities. The combination of transcriptional co-activation and actin nucleation activities suggests that JMY might mediate cellular decisions involving apoptosis and migration. Alternatively, JMY might be a chimaera whose transcriptional and

cytoskeletal functions are more or less independent. More intriguing is JMY's combination of Arp2/3-dependent and Arp2/3-independent nucleation activities. A cell switching from a resting to a motile state must remodel its cytoskeleton extensively¹⁶. The leading edge of most migrating cells is characterized by a highly branched dendritic arbour of actin filaments nucleated by Arp2/3, and one requirement for generating such a network is the pre-existence of 'mother' filaments for Arp2/3 to bind and branch from^{17,18}. Although resting cells contain some actin filaments (such as cortical actin or stress fibres), recent work suggests that not all filaments can serve as efficient substrates for Arp2/3-dependent nucleation^{19,20}. We propose that JMY contributes to cell motility by nucleating filaments to jump-start Arp2/3-dependent nucleation and branching. By first nucleating new mother filaments and then activating Arp2/3 to branch off these filaments, JMY could promote the rapid formation of a branched actin network. It is also possible that JMY has evolved to promote actin polymerization in different cellular contexts, either in the cytoplasm in the presence of Arp2/3, or in the nucleus in the absence of Arp2/3 (see model in Fig. 5h). For example, it would be interesting

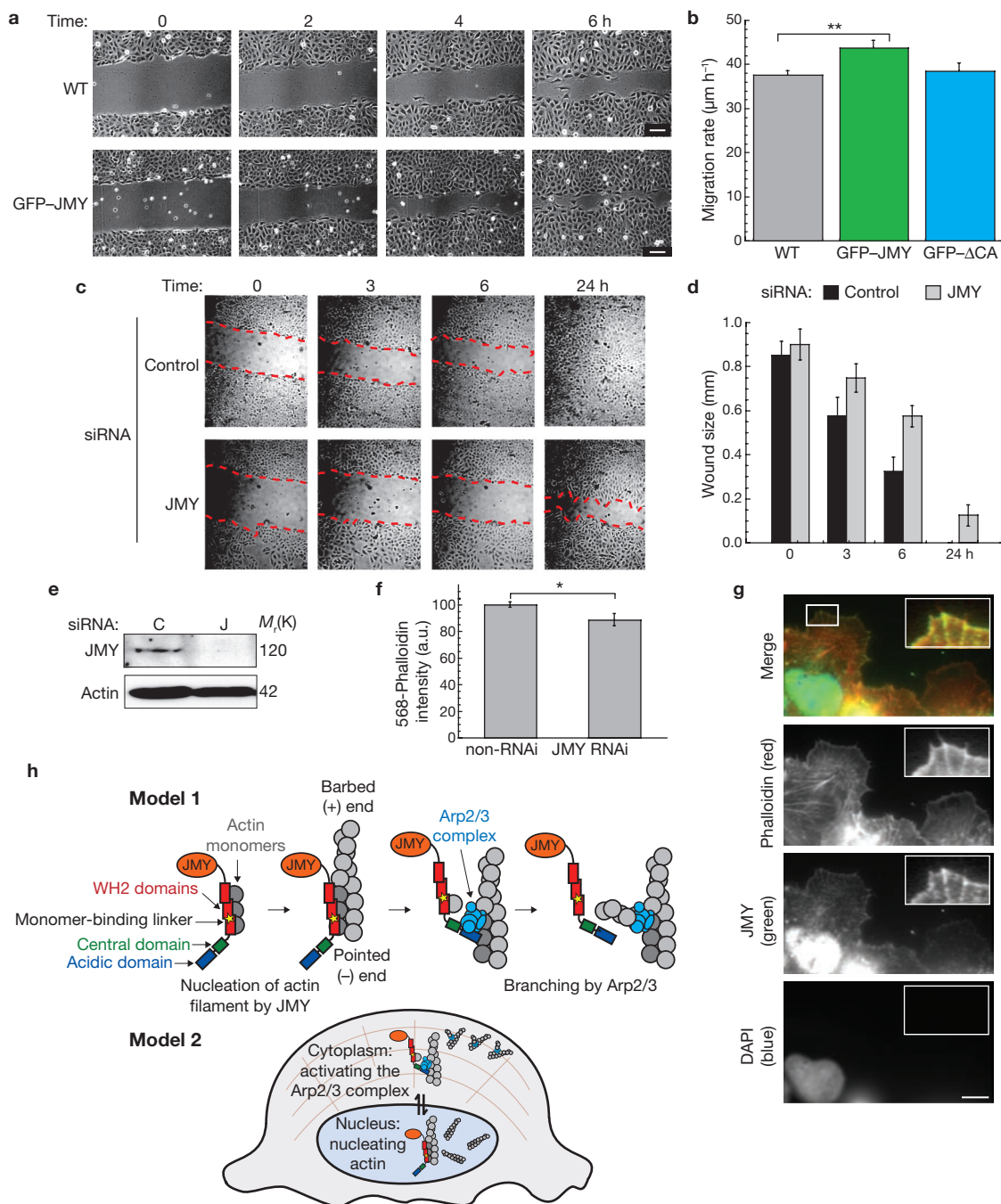


Figure 5 JMY contributes to cell motility. **(a, b)** Expressing GFP-JMY in U2OS cells significantly increases their motility in wound-healing assays. **(a)** Stable lines of GFP-JMY and GFP-JMY ΔCA were wounded by being scraped with micropipette tips. Images were acquired at 0, 2, 4, 6 and 12 h after wounding. Scale bars, 100 μm . **(b)** The migration rate from 0–6 h was averaged from a minimum of four replicates on each of three days. GFP-JMY expression induces cells to migrate 16.6% faster than wild-type cells ($n = 3$, $P < 0.003$). Cells expressing a truncation of JMY lacking the Arp2/3-interacting CA domain migrate at the same rate as wild-type cells. Error bars indicate s.e.m. **(c–e)** Wound-healing assays in U2OS cells indicate that knocking down JMY by RNAi impairs cell migration. Cells were transfected with JMY or control non-targeting 2 (Dharmacon) siRNA (C) and wounded (red dashed line) as in **a**. Images were taken at the same position 0, 3, 6 and 24 h after wounding. **(d)** Wound size at each time point for all conditions. ($n = 4$). Error bars indicate s.e.m. **(e)** Western blots show RNAi efficiency in U2OS cells. **(f)** Knocking down

JMY expression decreases cellular levels of F-actin. HEK 293 cells were transfected with a vector encoding both GFP and a JMY-specific shRNA²⁵, then fixed and stained with Alexa Fluor 568-phalloidin (568-phalloidin). The average phalloidin intensity in GFP-negative (non-RNAi-treated) and GFP-positive (RNAi-treated) cells is plotted ($n = 396$, $P < 0.03$; see Methods). Error bars indicate s.e.m. **(g)** JMY localizes to the leading edge of U2OS cells. Cells were grown as above, then fixed and stained for JMY 15 min after wounding. JMY is primarily nuclear, but it is also enriched at the leading edge (indirect immunofluorescence, green) where it co-localizes with a subset of actin filaments (Alexa Fluor 568-phalloidin, red). Inset: leading edge, contrast enhanced to show actin filaments and JMY. Scale bar, 10 μm . **(h)** Models of *in vivo* role of JMY. In model 1, JMY nucleates filaments that then serve as substrates for dendritic nucleation by Arp2/3. In model 2, JMY evolved to nucleate actin in different cellular contexts. In the nucleus it nucleates unbranched filaments, and in the cytoplasm it both nucleates filaments and activates Arp2/3.

to test whether inactivation of JMY's function in actin dynamics affects its role as a p300-dependent transcriptional co-activator for p53. Future work is aimed at testing these models. □

METHODS

Molecular biology and biochemistry. Constructs were cloned from full-length mouse JMY⁴, fly Spire² and rat N-WASp, with standard techniques. Primer sequences are available from the authors on request. All constructs were sequenced to ensure that no mutations were introduced during cloning. JMY fragments were expressed as glutathione S-transferase (GST) fusions in *Escherichia coli* and purified with a combination of glutathione and cation chromatography. Except for individual WH2 domains (Supplementary Information, Fig. S2), the GST was removed to prevent dimerization of the recombinant protein, which results in a marked increase in the rate of both intrinsic nucleation and activation of Arp2/3 (data not shown). To improve the reproducibility of fluorimetry reactions, we mutated the non-conserved cysteine C978 to serine. This mutation does not change the kinetics of activation of Arp2/3 (Supplementary Information, Fig. S6h, i) but results in a peptide that is more stable than the wild type. JMY concentrations were calculated from predicted molar extinction coefficients for JMY peptides that contained tryptophan residues (ProtParam), or by quantitative SDS-PAGE and staining with Sypro-Red (Invitrogen).

Actin polymerization assays. Actin was purified from *Acanthamoeba castellanii* as described²¹, labelled with pyrene iodoacetamide as described²², and stored on ice. Arp2/3 was purified from *Acanthamoeba* as described²³ and flash-frozen with 10% glycerol. For all assays, Arp2/3 was thawed daily and diluted with 1 mg ml⁻¹ BSA in buffer A (0.2 mM ATP, 0.5 mM tris(2-carboxyethyl)phosphine (TCEP), 0.1 mM CaCl₂, 0.02% w/v sodium azide, 2 mM Tris-HCl pH 8.0 at 4 °C). Actin polymerization assays were performed in 1 × KMEI (50 mM KCl, 1 mM MgCl₂, 1 mM EGTA, 10 mM imidazole pH 7.0). Ca²⁺-actin was converted into Mg²⁺-actin by incubating actin in 50 mM MgCl₂, 0.2 mM EGTA for 2 min before adding 10 × KMEI and test components. Pyrene fluorescence was measured with an ISS PCI/K2 fluorimeter. Unless otherwise noted, polymerization reactions contained 2 μM actin (labelled with 5% pyrene), 2.5 nM Arp2/3 and 167 nM JMY or N-WASp. JMY proteins were diluted with 10 mg ml⁻¹ BSA in buffer A to prevent loss of activity. To normalize fluorimetry data, we subtracted the offset from zero then divided by the plateau value of actin alone, so as to not mask the effects of sequestration by JMY. For half-time calculations, reactions were normalized by dividing by their own plateau and solving for time at half-maximal fluorescence (0.5 arbitrary units).

To reveal actin filaments we polymerized 2 μM actin under the same conditions as those used for fluorimetry, then arrested reactions at the times indicated with Alexa Fluor 488 phalloidin and Latrunculin B. This technique preserves the ratio of monomeric actin to filamentous actin at the moment of quenching²⁴. To keep the concentration of F-actin constant we arrested reactions at their individual $t^{9/10}$ (time at nine-tenths-maximal fluorescence, 0.9 arbitrary units) values: 1 min 40 s for JMY + Arp2/3, 6 min 20 s for Scar + Arp2/3, and 37 min 0 s for actin alone. Filaments were diluted to low nanomolar concentrations and spotted onto coverslips coated with poly-(L-lysine) (Sigma), using wide-bore pipette tips to minimize shearing.

Cell culture. U2OS (ATCC) and HEK 293 cells were cultured in DMEM medium supplemented with 10% FBS, 2 mM L-glutamine, non-essential amino acids, and penicillin-streptomycin (UCSF Cell Culture facility). For transfection, cells were seeded onto glass coverslips and transfected with haemagglutinin-tagged JMY⁴ using GeneJuice (Merck), or with GFP-JMY and GFP-RNAi constructs using Lipofectamine LTX (Invitrogen), in accordance with the manufacturer's protocol. HL-60 cells were cultured as described²⁵, in RPMI-1640 with 25 mM HEPES, 2.0 g l⁻¹ NaHCO₃, 10% FBS, 1% antibiotic-antimycotic (Fisher), and were passaged every three or four days to a density of 2×10^5 cells ml⁻¹. Differentiation was in complete medium containing 1.3% DMSO (Hybrimax; Sigma). All cells were grown at 37 °C with 5% CO₂. Primary human neutrophils were obtained by finger prick as described²⁶.

Immunofluorescence of HL-60 cells was performed as described²⁵. In brief, flamed coverslips were treated with 200 μg ml⁻¹ bovine plasma fibronectin (Sigma) in PBS, washed with PBS, and blocked with 1.8% low-endotoxin BSA (Sigma) in modified Hanks buffered saline solution (mHBSS: 150 mM NaCl, 4 mM KCl, 1 mM MgCl₂, 10 mM glucose, 20 mM HEPES pH 7.4 at 22 °C) for 5 min before

adhering cells. Cells were pelleted and resuspended in BSA/mHBSS, adhered to coverslips for 30–60 min at 37 °C, and then washed to remove unbound cells. Stimulation or mock stimulation was in BSA/mHBSS with 100 nM (HL-60s) or 20 nM (human neutrophils) fMLP, or DMSO (carrier), for 5 min at 22 °C. Cells were fixed in 3.2% formaldehyde in cytoskeletal buffer (138 mM KCl, 3 mM MgCl₂, 2 mM EGTA, 320 mM sucrose, 10 mM HEPES pH 7.2 at 22 °C). For immunofluorescence of U2OS cells, cells were plated on flamed, fibronectin-coated coverslips, and fixed for 30 min in 3.2% formaldehyde in PBS. Cells were then permeabilized with 0.1% Triton X-100 in PBS with 1.4 U ml⁻¹ Alexa Fluor 568-phalloidin (Invitrogen) to stabilize and reveal filaments. For JMY immunolocalization, rabbit polyclonal JMY antibody 1289 (ref. 5) or anti-haemagglutinin antibody HA11 (Babco) was used at 1:500 dilution. Alexa Fluor 488-labelled goat anti-rabbit secondary antibody (Invitrogen) was used at 1:500 dilution. 4,6-Diamidino-2-phenylindole (DAPI; Sigma) was used at 0.5 μg ml⁻¹. Samples were mounted with fluorescent mounting medium (DakoCytomation).

Epifluorescence and wide-field images were acquired on a Nikon TE300 inverted microscope equipped with a Hamamatsu C4742-98 cooled charge-coupled device camera, with Simple PCI software (Compix), using 100× and 60× 1.4 numerical aperture (NA) Plan Apo objectives (Nikon), or with a 10× 0.6 NA phase objective, using MicroManager software²⁷. For quantification of F-actin levels in cells expressing GFP-PWWCA or GFP, micrographs were acquired with an IX Micro automated microscope, using identical illumination conditions. Cells were identified and outlined by using ImageJ software, background was subtracted, and the average intensities in the red and green channels were measured. We used ImageJ (National Institutes of Health) and Adobe Photoshop (Adobe) for image analysis and contrast adjustment.

For wound-healing experiments, cells were plated on marked coverslips at the same density, scratch-wounded with a micropipette tip, washed to remove detached cells, and then given fresh medium and kept at 37 °C during image acquisition. Stable lines of U2OS cells stably expressing GFP-JMY and variants were selected in 500 μg ml⁻¹ G418 for at least three weeks, then enriched by fluorescence-activated cell sorting (FACS) (UCSF Flow Cytometry Core). siRNA was used at a final concentration of 25 nM (hJMY siRNA from Santa Cruz and control non-targeting 2 from Dharmacon) and transfected into cells with Oligofectamine or Dharmafect 1 (both in accordance with the manufacturer's protocols), and cells were grown for 72 h before experiments. To discriminate between cells treated with RNAi and cells not treated with RNAi, pL-UGIH plasmid (American Type Culture Collection) was modified to contain a human JMY-specific hairpin based on the sequence of JMY-specific siRNA-3 by the method of ref. 25. HEK 293 cells transiently transfected with this construct were grown for seven days before fixation or immunoblotting.

Standard methods were used for western blotting, using 1:500 1289 or 1:1,000 L-16 (Santa Cruz Biotechnology) JMY primary antibodies and 1:5,000 horseradish peroxidase (HRP)-labelled anti-rabbit secondary antibodies (Jackson ImmunoResearch). p300-CT primary antibody (Millipore) was used at 1:500, goat anti-human glyceraldehyde-3-phosphate dehydrogenase (Santa Cruz) was used at a dilution of 1:10,000, and mouse anti-human actin (Sigma) was used at 1:20,000. HRP-labelled secondary antibodies (Dako) were used at 1:10,000 dilution, and enhanced chemiluminescence reagent (SuperSignal West Pico; Pierce) was used in accordance with the manufacturer's instructions. All error values are s.e.m. We used two-tailed unpaired *t*-tests, assuming unequal variance, to calculate *P* values (Microsoft Excel).

Note: Supplementary Information is available on the Nature Cell Biology website.

ACKNOWLEDGEMENTS

We thank A. Kelly and R. Manlove for sequence analysis; O. Akin for help with Matlab scripts and advice; C. Campbell and H. Bourne for critical reading of the manuscript; and O. Weiner, S. Wilson, P. Temkin, E. Oh, C. Vizcarra, S. Cai, M. D'Ambrosio, K. Campellone, and members of the Mullins laboratory for reagents and helpful discussions. This work was supported by grants from the National Institutes of Health, the American Heart Association Predoctoral Fellowship (J.B.Z.), Medical Research Council funding (A.S.C.), and the Burroughs-Wellcome Fund Career Award in the Biomedical Sciences Fellowship (M.E.Q.).

AUTHOR CONTRIBUTIONS

J.B.Z., A.S.C. and M.E.Q. conducted the experiments and analysed the results. J.B.Z., A.S.C., M.E.Q., N.B.T. and R.D.M. conceived the experiments and wrote the manuscript.

COMPETING FINANCIAL INTERESTS

The authors declare that they have no competing financial interests.

Published online at <http://www.nature.com/naturecellbiology>

Reprints and permissions information is available online at <http://npg.nature.com/reprintsandpermissions/>

- Welch, M. & Mullins, R. Cellular control of actin nucleation. *Annu. Rev. Cell Dev. Biol.* **18**, 247–288 (2002).
- Quinlan, M. E., Heuser, J. E., Kerkhoff, E. & Mullins, R. D. *Drosophila* Spire is an actin nucleation factor. *Nature* **433**, 382–388 (2005).
- Marchand, J. B., Kaiser, D. A., Pollard, T. D. & Higgs, H. N. Interaction of WASP/Scar proteins with actin and vertebrate Arp2/3 complex. *Nature Cell Biol.* **3**, 76–82 (2001).
- Shikama, N. *et al.* A novel cofactor for p300 that regulates the p53 response. *Mol. Cell* **4**, 365–376 (1999).
- Coutts, A., Boulahbel, H., Graham, A. & La Thangue, N. Mdm2 targets the p53 transcription cofactor JMY for degradation. *EMBO Rep.* **8**, 84–90 (2006).
- Symons, M. *et al.* Wiskott–Aldrich syndrome protein, a novel effector for the GTPase CDC42Hs, is implicated in actin polymerization. *Cell* **84**, 723–734 (1996).
- Pollard, T. & Borisy, G. Cellular motility driven by assembly and disassembly of actin filaments. *Cell* **112**, 453–465 (2003).
- Cooper, J. & Pollard, T. Effect of capping protein on the kinetics of actin polymerization. *Biochemistry* **24**, 793–799 (1985).
- Pan, F., Egile, C., Lipkin, T. & Li, R. ARPC1/Arc40 mediates the interaction of the actin-related protein 2 and 3 complex with Wiskott–Aldrich syndrome protein family activators. *J. Biol. Chem.* **279**, 54629–54636 (2004).
- Ahuja, R. *et al.* Cordon-Bleu is an actin nucleation factor and controls neuronal morphology. *Cell* **131**, 337–350 (2007).
- Collins, S., Ruscetti, F., Gallagher, R. & Gallo, R. Normal functional characteristics of cultured human promyelocytic leukemia cells (HL-60) after induction of differentiation by dimethylsulfoxide. *J. Exp. Med.* **149**, 969–974 (1979).
- Kowalski, J. R. *et al.* Cortactin regulates cell migration through activation of N-WASP. *J. Cell Sci.* **118**, 79–87 (2005).
- Sablina, A., Chumakov, P. & Kopnin, B. Tumor suppressor p53 and its homologue p73 α affect cell migration. *J. Biol. Chem.* **278**, 27362–27371 (2003).
- Gadea, G., de Toledo, M., Anguille, C. & Roux, P. Loss of p53 promotes RhoA-ROCK-dependent cell migration and invasion in 3D matrices. *J. Cell Biol.* **178**, 23–30 (2007).
- Krubasik, D. *et al.* Absence of p300 induces cellular phenotypic changes characteristic of epithelial to mesenchyme transition. *Br. J. Cancer* **94**, 1326–1332 (2006).
- Southwick, F. S., Dabiri, G. A., Paschetto, M. & Zigmund, S. H. Polymorphonuclear leukocyte adherence induces actin polymerization by a transduction pathway which differs from that used by chemoattractants. *J. Cell Biol.* **109**, 1561–1569 (1989).
- Mullins, R., Heuser, J. & Pollard, T. The interaction of Arp2/3 complex with actin: nucleation, high affinity pointed end capping, and formation of branching networks of filaments. *Proc. Natl Acad. Sci. USA* **95**, 6181–6186 (1998).
- Blanchoin, L. *et al.* Direct observation of dendritic actin filament networks nucleated by Arp2/3 complex and WASP/Scar proteins. *Nature* **404**, 1007–1011 (2000).
- Blanchoin, L., Pollard, T. D. & Hitchcock-DeGregori, S. E. Inhibition of the Arp2/3 complex-nucleated actin polymerization and branch formation by tropomyosin. *Curr. Biol.* **11**, 1300–1304 (2001).
- Shao, D., Forge, A., Munro, P. & Bailly, M. Arp2/3 complex-mediated actin polymerization occurs on specific pre-existing networks in cells and requires spatial restriction to sustain functional lamellipod extension. *Cell Motil. Cytoskel.* **63**, 395–414 (2006).
- Gordon, D. J., Eisenberg, E. & Korn, E. D. Characterization of cytoplasmic actin isolated from *Acanthamoeba castellanii* by a new method. *J. Biol. Chem.* **251**, 4778–4786 (1976).
- Cooper, J. A., Walker, S. B. & Pollard, T. D. Pyrene actin: documentation of the validity of a sensitive assay for actin polymerization. *J. Muscle Res. Cell Motil.* **4**, 253–262 (1983).
- Dayel, M. J., Holleran, E. A. & Mullins, R. D. Arp2/3 complex requires hydrolyzable ATP for nucleation of new actin filaments. *Proc. Natl Acad. Sci. USA* **98**, 14871–14876 (2001).
- Akin, O. & Mullins, R. D. Capping protein increases the rate of actin-based motility by promoting filament nucleation by the Arp2/3 complex. *Cell* **133**, 841–851 (2008).
- Weiner, O. *et al.* Hem-1 complexes are essential for Rac activation, actin polymerization, and myosin regulation during neutrophil chemotaxis. *PLoS Biol.* **4**, e38 (2006).
- Cassimeris, L., McNeill, H. & Zigmund, S. Chemoattractant-stimulated polymorphonuclear leukocytes contain two populations of actin filaments that differ in their spatial distributions and relative stabilities. *J. Cell Biol.* **110**, 1067–1075 (1990).
- Stuurman, N., Amodaj, N., Vale, R. D. Micro-Manager: open source software for light microscope imaging. *Microsc. Today* **15**, 42–43 (2007).
- Petrella, E., Machesky, L., Kaiser, D. & Pollard, T. Structural requirements and thermodynamics of the interaction of proline peptides with profilin. *Biochemistry* **35**, 16535–16543 (1996).
- Kelly, A., Kranitz, H., Dötsch, V. & Mullins, R. Actin binding to the central domain of WASP/Scar proteins plays a critical role in the activation of the Arp2/3 complex. *J. Biol. Chem.* **281**, 10589–10597 (2006).
- Kreishman-Deitrick, M. *et al.* NMR analyses of the activation of the Arp2/3 complex by neuronal Wiskott–Aldrich syndrome protein. *Biochemistry* **44**, 15247–15256 (2005).
- Campellone, K. G., Webb, N. J., Znameroski, E. A. & Welch, M. D. WHAMM is an Arp2/3 complex activator that binds microtubules and functions in ER to Golgi transport. *Cell* **134**, 148–161 (2008).

DOI: 10.1038/ncb1852

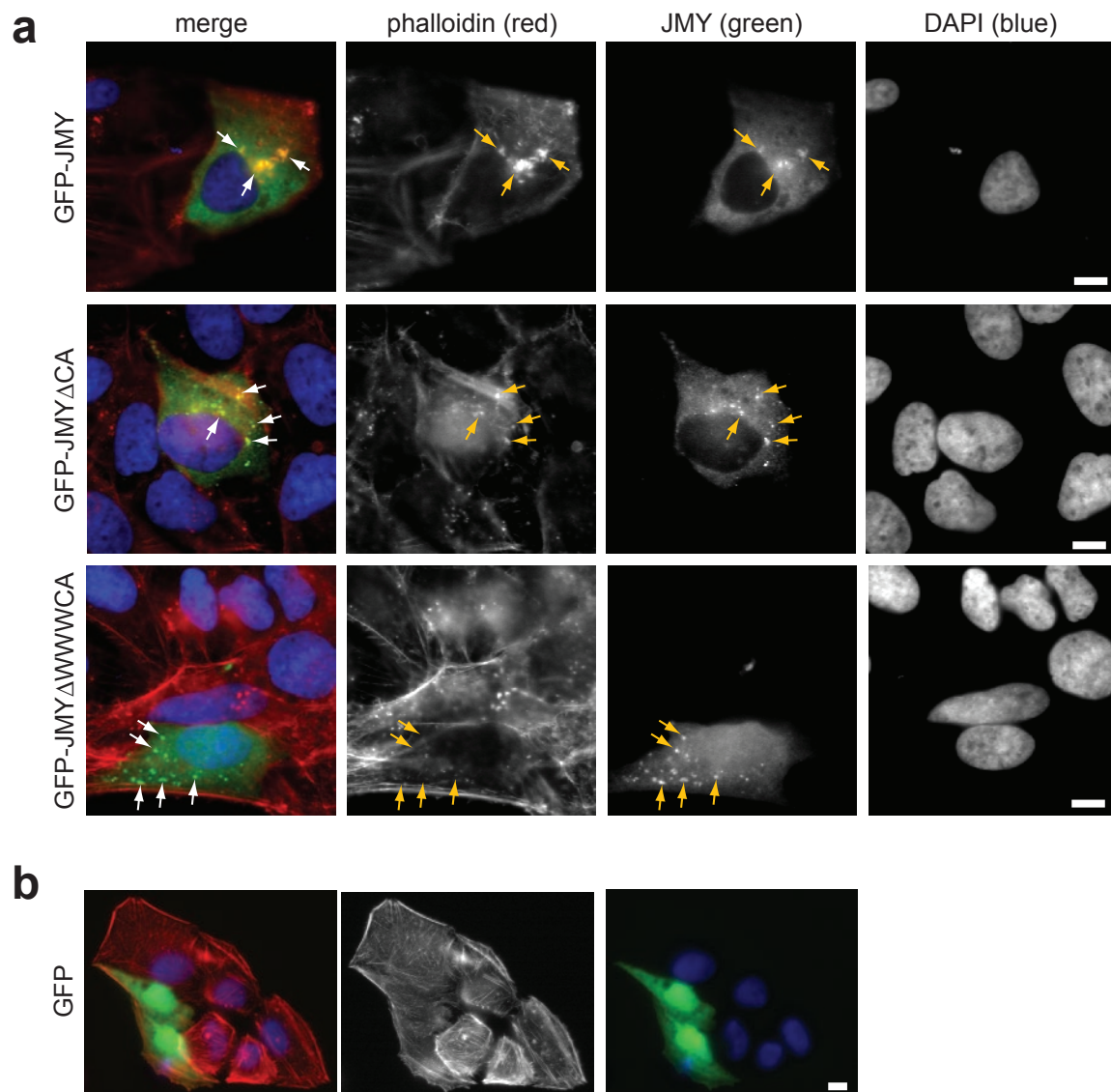
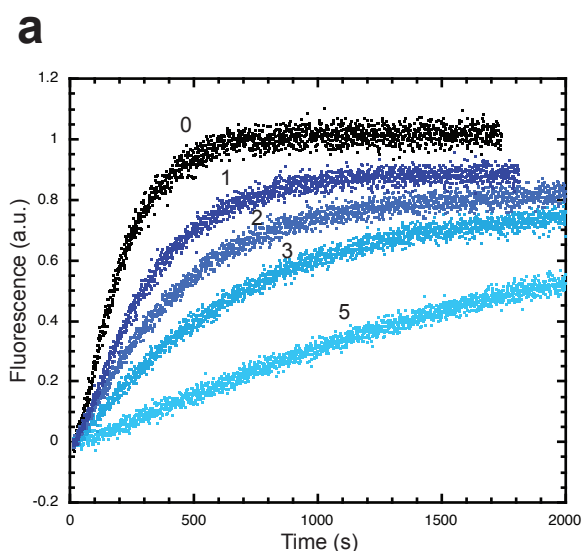


Figure S1 Expression of GFP-JMY in U2OS cells. **a**, Expression of GFP-JMY (top panels), GFP-JMY Δ CA (center panels), and GFP-JMY Δ WWWCA (bottom panels) in U2OS cells. Cells were fixed and stained with Alexa Fluor 568 phalloidin (red) and DAPI (blue). All JMY constructs localize to cytoplasmic

clusters (arrowheads) in addition to being diffuse in the cytoplasm. Ectopic filamentous actin structures colocalize with GFP-JMY and GFP-JMY Δ CA, but not GFP-JMY Δ WWWCA. **b**, Expression of GFP in U2OS cells. (Compare to expression of GFP-PWWWCA in Fig. 1). Scale bars, 20 μ m.



JMY Wa	<i>M. musculus</i>	AAHLFDSSQLVSAKKLRKT
	<i>B. taurus</i>	SAHLFDSSQLVSAKKLRKT
	<i>H. sapien</i>	SAHLFDSSQLVSAKKLRKT
	<i>X. tropicalis</i>	LAQLFDSSQLLNARKTLKKT
	<i>D. rerio</i>	SARFFDSSQLLNARKLRKT
	<i>T. nigroviridis</i>	SPRFFDSSQLQTAARKLRKT
	<i>C. familiaris</i>	SAHLFDSSQLVSAKKLRKT
JMY Wb	<i>M. musculus</i>	SPMDEVLASLKRGSFHLKVV
	<i>R. norvegicus</i>	SPMDEVLASLKRGSFHLKVV
	<i>H. sapien</i>	SPMDEVLASLKRGSFHLKVV
	<i>X. tropicalis</i>	SPMDEVLASLKRGSFHLKVV
	<i>D. rerio</i>	SPMDEVLASLKRGSFHLRKA
	<i>P. troglodytes</i>	SPMDEVLASLKRGSFHLKVV
	<i>C. familiaris</i>	SPMDEVLASLKRGSFHLKVV
WHAMM W1	<i>M. musculus</i>	GSMDEVLASLRQGKASLRKV
	<i>H. sapien</i>	GSMDEVLASLRHGRAPLRKV
JMY Wc	<i>M. musculus</i>	DDSNNILAQIRKGVK-LKKV
	<i>R. norvegicus</i>	DDSNNILAQIRKGVK-LKKV
	<i>H. sapien</i>	DDSNNILAQIRKGVK-LKKV
	<i>X. tropicalis</i>	DESNNILAQIRKGVK-LKKV
	<i>D. rerio</i>	DDGNNILAQIRKGVK-LRKV
	<i>P. troglodytes</i>	DDSNNILAQIRKGVK-LKKV
	<i>C. familiaris</i>	DDSNNILAQIRKGVK-LKKV
WHAMM W2	<i>M. musculus</i>	SVNEQVLAATIRQGVQ-LKKV
	<i>H. sapien</i>	SINEHILAAITRQGVK-LKKV

Figure S2 Wa, Wb, and Wc are *bona fide* WH2 domains. **a**, 10 μ M actin was polymerized with increasing concentrations of GST-W_a in KMEI (see Methods). GST-W_a concentrations are indicated (in μ M). Traces are normalized relative to 10 μ M actin alone so as to not mask the effect of sequestration. Inhibition of spontaneous polymerization is evidence that these WH2 domains bind monomeric actin. GST-W_b and GST-W_c also inhibit

b

Spire A	<i>M. musculus</i> Spire-1	ARFWVQVMRDLRNGVKLKKV
	<i>R. norvegicus</i> Spire-1	ARFWVQVMRDLRNGVKLKKV
	<i>H. sapien</i> Spire-1	ARFWVQVMRDLRNGVKLKKV
	<i>X. laevis</i> Spire	GNLWSNVIKELRLGIRLRNS
	<i>M. musculus</i> Spire-2	ARLWVQLMRELRRHGVLKVV
	<i>R. norvegicus</i> Spire-2	ARLWVQLMRELRRHGVLKVV
	<i>H. sapien</i> Spire-2	ARLWVQLMRELRRGVKLKVV
<i>D. melanoga ster</i> Spire	ARFWVQVIDELRRGVRLKKS	
Spire B	<i>M. musculus</i> Spire-1	TPYEMLMDDIRCKRYTLRKKV
	<i>R. norvegicus</i> Spire-1	TPYEMLMDDIRCKRYTLRKKV
	<i>H. sapien</i> Spire-1	TPYEMLMDDIRCKRYTLRKKV
	<i>X. laevis</i> Spire	TPTELLMNDIRAKRYTLREEV
	<i>M. musculus</i> Spire-2	TPTEMLMQDIRARNYKLRKKV
	<i>R. norvegicus</i> Spire-2	TPTEMLMQDIRARNYKLRKKV
	<i>H. sapien</i> Spire-2	TPTEMLMQDIRARNYKLRKKV
<i>D. melanoga ster</i> Spire	TPYEILMQDIRAKKYQLRKKV	
Spire C	<i>M. musculus</i> Spire-1	KSAHEVILDFIRSRPPLNPA
	<i>R. norvegicus</i> Spire-1	KSAHEIILDFIRSRPPLNPA
	<i>H. sapien</i> Spire-1	KSAHEIILDFIRSRPPLNPA
	<i>X. laevis</i> Spire	QSVENFIMDFIRSQPLRPA
	<i>M. musculus</i> Spire-2	KDAHELILDFIRSRPPLKQV
	<i>R. norvegicus</i> Spire-2	KDAHELILDFIRSRPPLKQV
	<i>H. sapien</i> Spire-2	KDAHELILDFIRSRPPLKQV
<i>D. melanoga ster</i> Spire	KDAHAMILEFIRSRPPLKKA	
Spire D	<i>M. musculus</i> Spire-1	SLHERILEETKAEK-LRPV
	<i>R. norvegicus</i> Spire-1	SLHERILEETKAEK-LRPV
	<i>H. sapien</i> Spire-1	SLHERILEETKAEK-LRPV
	<i>X. laevis</i> Spire	SLHELIMSEIKSGKK-LRST
	<i>M. musculus</i> Spire-2	TLHEKILEETKQERR-LRPV
	<i>R. norvegicus</i> Spire-2	TLHEKILEETKQERR-LRPV
	<i>H. sapien</i> Spire-2	SLHEKILEETKQERR-LRPV
<i>D. melanoga ster</i> Spire	SPREQLMESIRKKGKE-LKQI	
Others	<i>H. sapien</i> N-WAS p Wa	GNKAALLDQIREGAQ-LKKV
	<i>M. musculus</i> N-WAS p Wa	GNKAALLDQIREGAQ-LKKV
	<i>H. sapien</i> N-WAS p Wb	SGRDALLDQIRQGIQ-LKSV
	<i>M. musculus</i> N-WAS p Wb	SGRDALLDQIRQGIQ-LKSV
	<i>H. sapien</i> Scar-1	DARSVLLAETIRKGIQ-LRKV
	<i>H. sapien</i> Scar-3	DARSDLLAETIRMGIQ-LKKV
	<i>D. melanoga ster</i> Scar	DPNDLMKAITRDGIT-LRKV
<i>M. musculus</i> Cobl W1	HSALMEATHSSGGREKLRKV	
<i>M. musculus</i> Cobl W2	RSALLAETIRGHSGTLSLRKV	
<i>M. musculus</i> Cobl W3	RQALMDAETIRSGTGAAKLRKV	

spontaneous polymerization (not shown). **b**, Alignment of WH2 domains from Spire, JMY, WHAMM, Cordon Bleu, and WASp-family proteins (ClustalW). Conserved hydrophobic residues are highlighted gray, and conserved basic residues are highlighted red. JMY WH2 domains were identified by searching genome databases using a consensus WH2 domain sequence derived from a combination of sequence conservation, structural, and biochemical criteria.

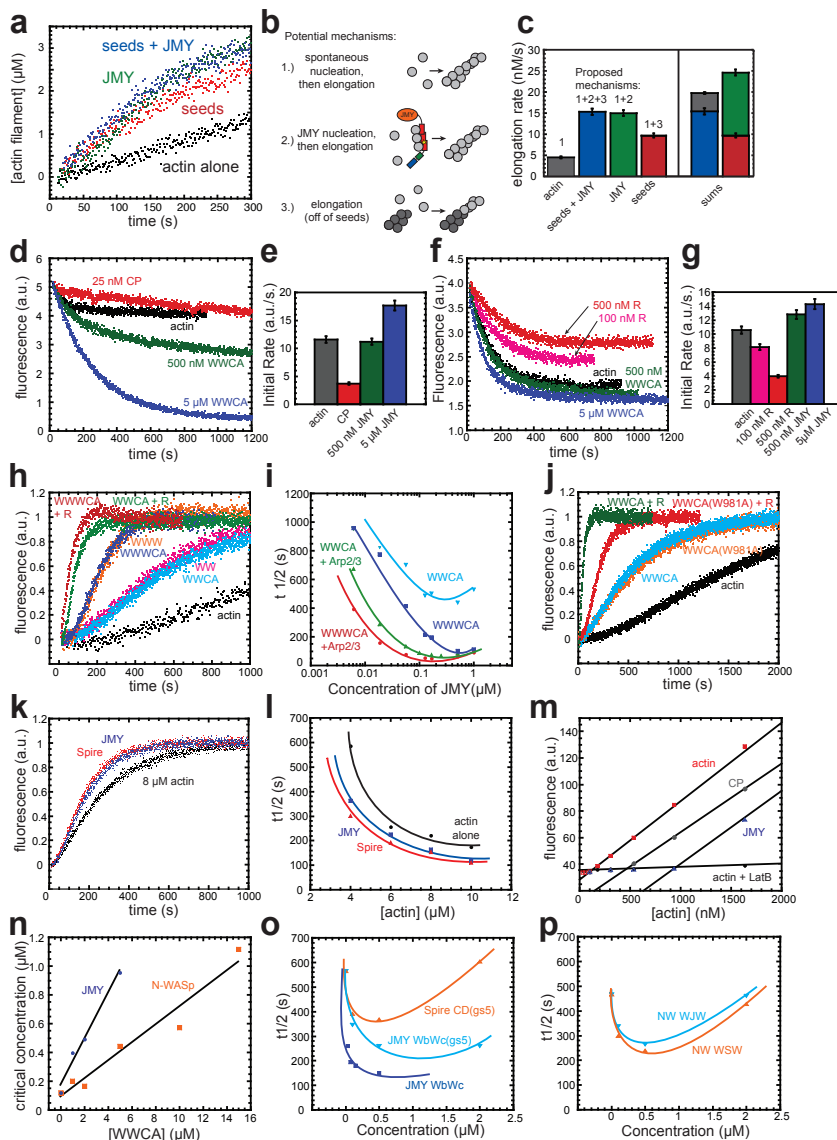


Figure S3 Biochemical characterization of JMY. **a-c**, JMY does not affect elongation of preformed filaments. 4 μM actin was polymerized alone or in the presence of preformed actin filament seeds, with or without 500 nM JMY WWCA (as noted). Polymerization rates were calculated during the linear phase of the reactions, between 40 and 180 s. **b**, Cartoon depicting the three types of reactions occurring in the experiments. Experiments containing JMY and seeds represent a combination of all three reactions: (1) nucleation by JMY, (2) elongation off of pre-existing seeds, and (3) background spontaneous polymerization of actin. **c**, Quantification of polymerization rates. Left: elongation rates for reactions. Right: stacked columns indicate that reactions containing seeds and JMY (left bar) are slower than the sum of JMY-nucleation plus seed elongation alone (right bar). This is consistent with the increased rate of polymerization in the presence of JMY being due to increased nucleation, not increased rate of elongation or filament severing. Spontaneous polymerization of actin also contributes to the observed rate of polymerization. To account for this reaction being represented twice in the bars on the right, we added this rate onto the left bar for reference (light gray, actin alone). Error bars, s.e.m.; $n=4$. **d-e**, JMY WWCA does not cap the barbed ends of actin filaments. Capping protein slows depolymerization from the barbed end of actin filaments, whereas JMY does not. Increased rate of depolymerization at high concentrations of JMY (consistent with Spire results¹) is likely due to sequestration of actin monomers by JMY. Initial rate of depolymerization for reactions is plotted in **e**. Error bars, s.e.m.; $n=3$. **f-g**, JMY WWCA does not cap the pointed ends of gelsolin-capped actin filaments. The Arp2/3 complex binds to the pointed end of actin filaments, and slows pointed end

depolymerization, whereas JMY does not. Initial rate of depolymerization for reactions is plotted in **g**. Error bars, s.e.m.; $n=3$. **h-i**, JMY fragments composed of the two C-terminal WH2 domains (W_b and W_c) nucleate actin, but maximal activity requires all three WH2 domains. Similarly, reactions with WWWCA and Arp2/3 (red) are faster than those with WWCA and Arp2/3 (green). **i**, Dose curves of nucleation and activation of the Arp2/3 complex by JMY WWWCA (as in Fig. 1f) and JMY WWCA. **j**, Conserved tryptophan in the JMY acidic domain is important for activating the Arp2/3 complex, but not for JMY's intrinsic nucleation. This is consistent with JMY activating the Arp2/3 complex by the same mechanism as WASp-family proteins, and agrees with our results using WWW and W_bW_c , which indicate that only JMY WH2 domains contribute to nucleation. Experimental conditions as in Fig. 1c. **k-l**, Nucleation by JMY and Spire displays similar kinetics over a range of actin concentrations. Pyrene-actin polymerization assays with 167 nM JMY W_bW_c or Spire CD and increasing concentrations of actin. Reactions containing 8 μM actin are shown in **a**. Time to half-maximal fluorescence ($t_{1/2}$) was calculated as in Fig. 1d. **m-n**, Critical concentration experiments. Pyrene-actin was polymerized and diluted into KMEI, alone (red) or containing Latrunculin B (black), 60 nM capping protein (gray), or 5 μM JMY (blue). Fluorescence was measured after 14–18 hours. **n**, Critical concentration plotted as a function of concentration of JMY WWCA (blue) or N-WASp WWCA (orange). Like Spire¹, JMY WWCA weakly sequesters actin monomers, and N-WASp sequesters even more weakly. **o-p**, Dose-curves of loss of function (**o**) and gain of function (**p**) mutations presented in Fig. 3. Time to half-maximal fluorescence ($t_{1/2}$) is plotted, over a range of concentrations, for each construct.

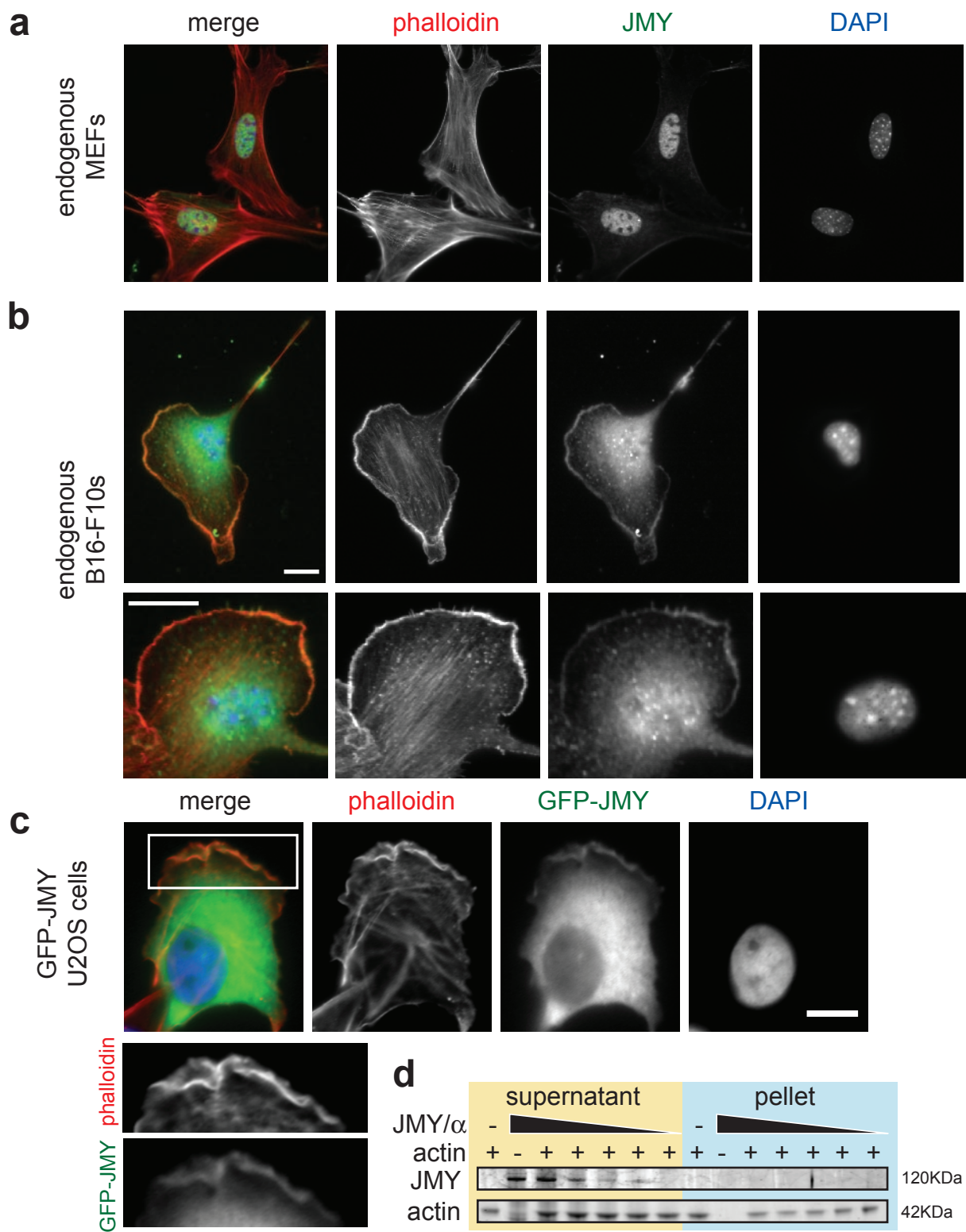


Figure S4 Localization of JMY. **a**, JMY is primarily nuclear in multiple cell types. MEFs were fixed and imaged by indirect immunofluorescence with anti-JMY antibody 1289 as in Fig. 4 (green in merged image). Filamentous actin was visualized with Alexa Fluor 568 phalloidin (red). DNA was visualized with DAPI (blue). **b**, In ruffling B16-F10 mouse melanoma cells, cytoplasmic JMY localizes to the leading edge. Two examples are shown. **c**, GFP-JMY expression in spreading U2OS cells. The majority of GFP-JMY is

cytoplasmic, but a fraction colocalizes with actin filaments at the leading edge. The box highlights the region expanded in bottom panels. Scale bars, 10 μ m. **d**, Full-length, his-tagged JMY does not copellet with actin filaments. Actin was polymerized in 1x KMEI and incubated with serial dilutions of JMY or buffer alone, then actin filaments were pelleted. Gel shows supernatants (left) and pellets (right) of actin alone, JMY alone, and 5 serial dilutions of JMY.

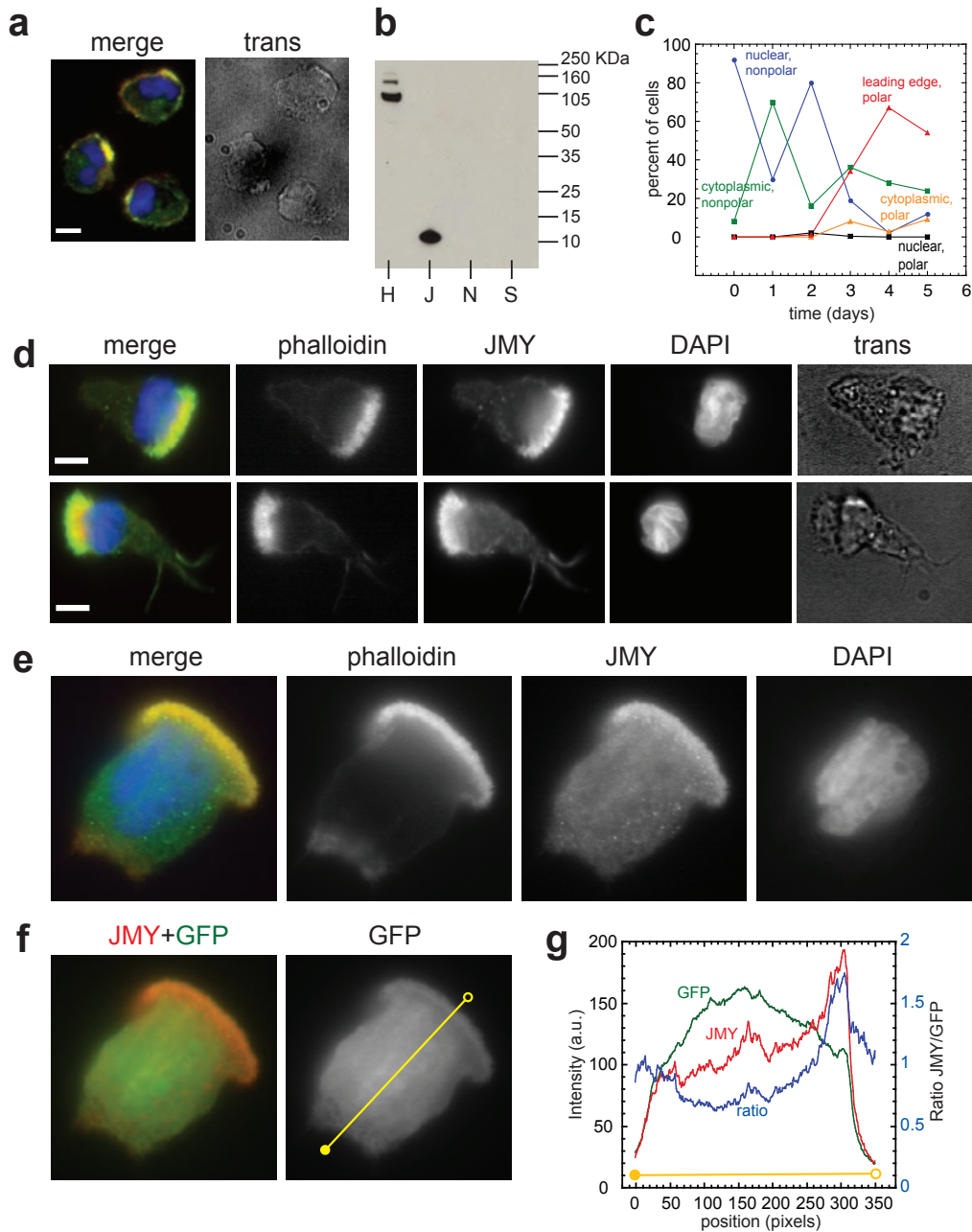


Figure S5 JMY in HL-60 cells and human neutrophils. **a, d**, Examples of human neutrophils (**a**) and HL-60 cells (**d**) stimulated with fMLP, as in Fig. 4. Micrographs show merged epifluorescence image, phalloidin (red), endogenous JMY (green), and DAPI. Transillumination micrographs are shown for reference. **b**, Western blot of JMY in high speed supernatants of cytosol from undifferentiated HL-60 cells (H) recognizes a single, major band with an apparent molecular weight of 110 kDa, consistent with the predicted molecular weight of JMY. The antibody recognizes purified JMY WWCA (J), but not N-WASP WWCA (N) or Scar WCA (S), demonstrating that it is specific for JMY. **c**, HL-60 cells were differentiated with 1.3% DMSO. At various time points cells were removed from the differentiating population, stimulated with fMLP, and immediately fixed and stained as in Fig. 5. JMY localization was scored as either mostly nuclear, mostly cytoplasmic, or at

the leading edge; and cell morphology was scored as nonpolar or polar, based on phalloidin staining of actin filaments. Cartoon on the right depicts the different classes of cells plotted in the graph. Note that JMY begins to leave the nucleus on the first day of differentiation, and cells begin to polarize in response to fMLP by the third day. **e-g**, We fixed and stained differentiated, stimulated HL-60 cells that expressed GFP (kind gift of O. Weiner, UCSF) for endogenous JMY, using Alexa Fluor 647 anti-rabbit secondary (Invitrogen). **e** shows a representative cell with JMY colocalized with actin filaments at the leading edge, as in Fig 4c. **f** shows GFP and JMY in the same cell. **g**, intensity was measured along the line shown in **f**, from the closed circle to the open circle, and plotted as a function of position (NIH ImageJ). The ratio of JMY to GFP was overlaid (blue), demonstrating that JMY is enriched relative to GFP at the leading edge of the cell.

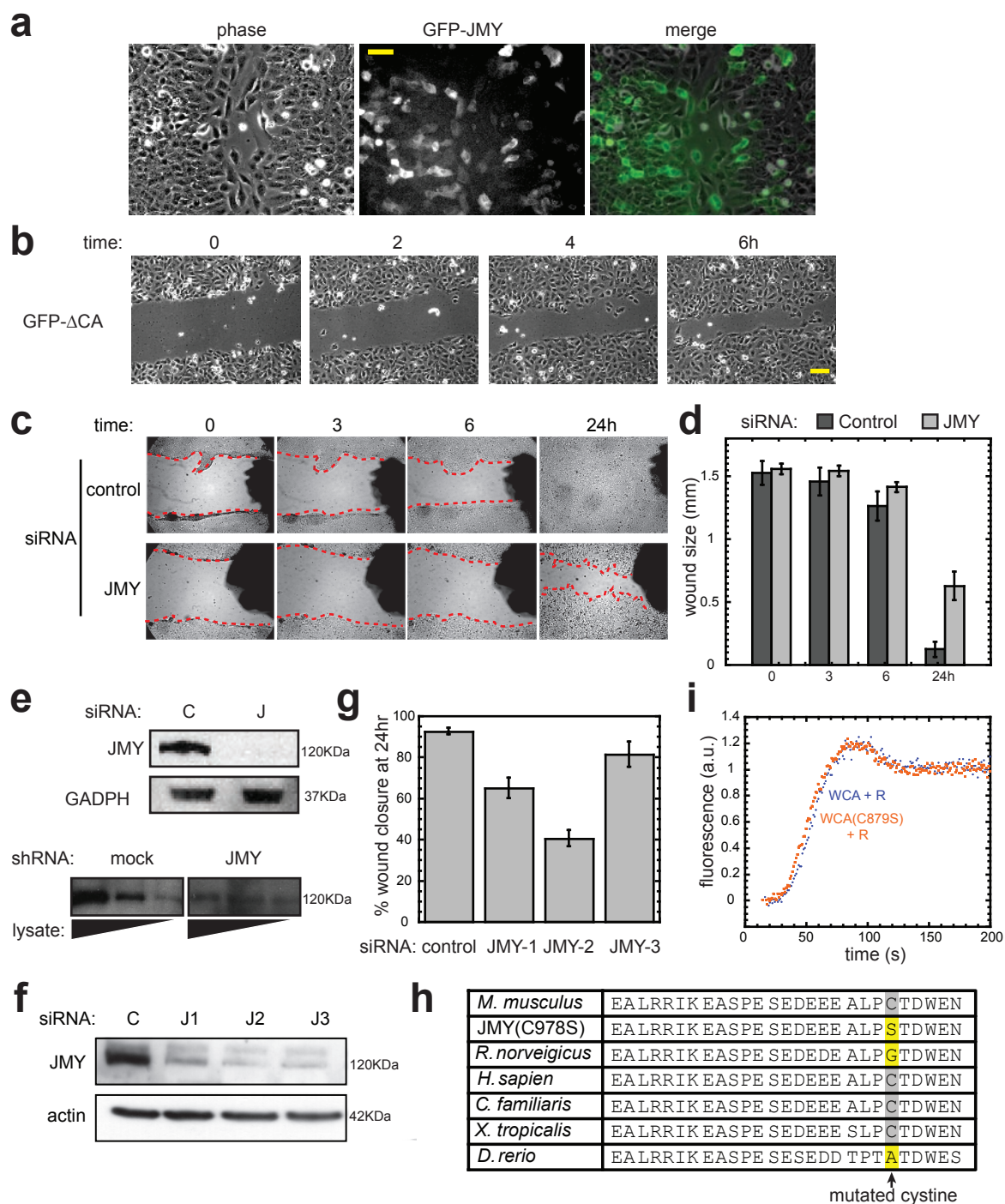


Figure S6 JMY contributes to cell migration. **a**, GFP-JMY expression in U2OS cells used in wound healing assays (Fig. 5). Cells were FACS sorted for purity, seeded at 900 thousand cells per well of a 12 well plate, grown overnight, then scratch-wounded with a pipette tip. Micrograph shows wounded cells in phase (left), epifluorescence (center), and merged (right). Scale bar, 100 μ m. **b**, U2OS cells expressing GFP-JMY Δ CA migrate at the same rate as wild-type cells. Phase contrast images of a representative wound healing assay quantified in Fig. 5. Scale bar, 100 μ m. **c-d**, Wound healing assays in HEK 293 cells indicate that knocking-down JMY by RNAi impairs cell migration. (Conditions as in Fig. 5; n=7). **e-f**, Western blots show RNAi efficiency in HEK 293 cells, using pooled siRNAs as in Fig 5 (e, top panel), shRNA plasmid (e, bottom panel, serial dilutions of cell lysate)

or individual siRNAs (f). C, control non-targeting 2 (Dharmacon) siRNA. Mock, shRNA empty vector **g**, Quantification of wound closure after 24 hours in HEK 293 cells treated with individual JMY siRNAs (JMY-1, JMY-2, JMY-3) or control siRNA. Knockdown of JMY expression with all three siRNAs cause a wound healing defect. **h-i**, Mutating nonconserved cysteine 978 to serine has no effect on Arp2/3 activation by JMY WCA. **h**, Alignment of JMY acidic domains shows that cysteine 978 is poorly conserved in available sequences (ClustalW). **i**, Activation of the Arp2/3 complex by JMY WCA and WCA(C978S) display identical kinetics after a day-long purification. After this time, the activity of WCA decreases quickly, while the activity of WCA(C978S) is stable for several days-weeks. Experimental conditions as in Fig. 1c.

Supplementary Information

p53-cofactor JMY is a Multifunctional Actin Nucleation Factor

J. Bradley Zuchero¹, Amanda S. Coutts², Margot E. Quinlan¹, Nicholas B. La Thangue², and R. Dyche Mullins¹

Supplementary Methods

Molecular biology. Amino acid numbers (mouse JMY, fly Spire, rat N-WASp) of constructs are: W_a, 853-876; W_b, 883-907; W_c, 913-938; WWWCA, 853-983; WWCA, 883-983; WCA, 906-983; W_bW_c, 883-938; W_aW_bW_c, 819-938; Spire CD, 428-482; N-WASp WWCA, 400-501; N-WASp WW, 400-450; GFP- and HA-JMY, 1-983; GFP-JMYΔCA, 1-938; GFP-JMYΔWWWCA, 1-852.

Actin biochemistry. For actin filament cosedimentation assays, we expressed His-tagged full length JMY in *E. coli*, purified it by affinity chromatography, and performed actin filament cosedimentation assays as described in Quinlan et al. (2007)² with minor modifications. Briefly, 4 μM actin was polymerized in 1x KMEI, 20 μg/mL BSA (loading control), and 1 mM DTT for one hour. An equal volume of serial dilutions of full length JMY was added to the actin. JMY was pre-cleared by centrifugation at 100,000 g for 20 min at 4° C before each assay. Samples were mixed, held on ice for 10 min, and pelleted at 100,000 g for 30 min at 4° C. Supernatants were removed, pellets were washed before resuspending, and each was analyzed by SDS-PAGE. We used SyproRed staining

(Invitrogen) and quantified gels using a multiformat imager (Typhoon 9400, GE Healthcare) and ImageQuant software (GE Healthcare).

Depolymerization and critical concentration assays were performed as described¹. Briefly, for barbed end depolymerization, we polymerized 5 μM actin (40% pyrene labelled) for at least one hour. To stimulate depolymerization, we diluted these filaments tenfold (to 500 nM) in 1x KMEI containing the proteins to be tested. Depolymerization is due to filaments disassembling until they reach a new steady state. Under these conditions depolymerization proceeds both from the barbed and pointed ends but dissociation of monomers from the barbed end is roughly 25 times faster than from the pointed end (ADP actin)³. The depolymerization rate we measure is, therefore, mostly dependent on the kinetics of the barbed end.

For pointed-end depolymerization experiments we made gelsolin-actin seeds by mixing 24 μM actin, 12 μM gelsolin, and 10 mM CaCl_2 in Buffer A and polymerizing for 4 hours at room temperature followed by incubation overnight at 4° C⁴. The concentration of pointed ends was quantified by actin elongation experiments. We made labelled filaments with capped barbed ends by polymerizing 5 μM actin (40% pyrene labelled) in the presence of 30 nM gelsolin-actin seeds. To stimulate depolymerization, we diluted these capped filaments tenfold (to 500 nM) in 1x KMEI containing proteins to be tested. To ensure that filament barbed ends were capped, we measured depolymerization kinetics in the presence of 500 nM Arp2/3, which caps free pointed ends.

Elongation experiments were performed as described.¹ Briefly, seeds were prepared by polymerizing 4 μM unlabeled actin in 1x KMEI for 1 hour at 22°C. 4 μM actin (5% pyrene labelled) was then polymerized alone or in the presence of these actin filament seeds, with or without 500 nM JMY WWCA (as noted). Polymerization rates were calculated during the linear phase of the reactions, between 40 and 180 s.

1. Quinlan, M. E., Heuser, J. E., Kerkhoff, E. & Mullins, R. D. *Drosophila* Spire is an actin nucleation factor. *Nature* 433, 382-8 (2005).
2. Quinlan, M., Hilgert, S., Bedrossian, A., Mullins, R. & Kerkhoff, E. Regulatory interactions between two actin nucleators, Spire and Cappuccino. *J. Cell Biol.* 179, 117-28 (2007).
3. Pollard, T. D. Rate constants for the reactions of ATP- and ADP-actin with the ends of actin filaments. *J Cell Biol* 103, 2747-54 (1986).
4. Mullins, R., Heuser, J. & Pollard, T. The interaction of Arp2/3 complex with actin: nucleation, high affinity pointed end capping, and formation of branching networks of filaments. *Proc. Natl. Acad. Sci. U.S.A.* 95, 6181-6 (1998).